SEMICONDUCTORS

Near-infrared–to–visible highly selective thermal emitters based on an intrinsic semiconductor

Takashi Asano,[1]*† Masahiro Suemitsu,[1,2†] Kohei Hashimoto,[1] Menaka De Zoysa,[1,3] Tatsuya Shibahara,[1] Tatsunori Tsutsumi,[1] Susumu Noda[1]

Control of the thermal emission spectra of emitters will result in improved energy utilization efficiency in a broad range of fields, including lighting, energy harvesting, and sensing. In particular, it is challenging to realize a highly selective thermal emitter in the near-infrared–to–visible range, in which unwanted thermal emission spectral components at longer wavelengths are significantly suppressed, whereas strong emission in the near-infrared–to–visible range is retained. To achieve this, we propose an emitter based on interband transitions in a nanostructured intrinsic semiconductor. The electron thermal fluctuations are first limited to the higher-frequency side of the spectrum, above the semiconductor bandgap, and are then enhanced by the photonic resonance of the structure. Theoretical calculations indicate that optimized intrinsic Si rod-array emitters with a rod radius of 105 nm can convert 59% of the input power into emission of wavelengths shorter than 1100 nm at 1400 K. It is also theoretically indicated that emitters with a rod radius of 190 nm can convert 84% of the input power into emission of <1800-nm wavelength at 1400 K. Experimentally, we fabricated a Si rod-array emitter that exhibited a high peak emissivity of 0.77 at a wavelength of 790 nm and a very low background emissivity of <0.02 to 0.05 at 1100 to 7000 nm, under operation at 1273 K. Use of a nanostructured intrinsic semiconductor that can withstand high temperatures is promising for the development of highly efficient thermal emitters operating in the near-infrared–to–visible range.

INTRODUCTION

Control of the thermal emission spectra of emitters has attracted considerable research attention because this will result in an improvement in energy utilization efficiency, which is required in a broad range of fields, including lighting (*1*), energy harvesting (*2*), and sensing (*3*). For example, emitters exhibiting strong thermal emission in a desired wavelength range with low background emission (*3*–*16*) are very useful as efficient light sources for sensing and illumination. For highly efficient (solar-) thermophotovoltaic (S-TPV) energy conversion, it is essential to limit the emission spectrum to a range just below the bandgap wavelength of the target photovoltaic cell (*17*–*22*). Control of emissivity/absorptivity spectra is also effective in radiative cooling applications (*23*).

To obtain improved energy utilization efficiency, it is important to suppress the unused spectral component of the thermal emission to close to zero while enhancing the required component close to the blackbody limit. However, establishing this control in the near-infrared–to–visible range is difficult. To date, nanostructured refractory metal emitters have been used to achieve this goal (*17*–*22*). These emitters selectively enhance the target wavelength component of the broadband emission of free carriers, on the basis of the photonic resonance of the nanostructure. However, it is difficult to suppress longer-wavelength emission using this strategy because thermally fluctuating free carriers essentially exhibit broad emission. Recently, the utilization of highly doped semiconductors instead of refractory metals has been proposed as a means of controlling the intensity of free-carrier absorption in emitters to increase the *Q* factors of the photonic resonances (*24*). Although this emitter design has succeeded in yielding a narrower emission line at near-infrared wavelengths, this approach continues to suffer from strong background emission due to free carriers in the longer-wavelength range. A third, alternative approach that has also been discussed is the use of a metal filament surrounded by a wavelength-selective mirror (*13*–*16*). In the study by Ilic *et al.* (*16*), for example, a theoretical calculation indicates that longer-wavelength emission can be successfully returned to the filament by optimized mirrors, resulting in a theoretical luminous efficiency of 40%. However, background emission remains apparent in the experimental application demonstrated by Ilic *et al.* (*16*), and the difference between the visible peak intensity and the average intensity of the longer-wavelength components remains at ~3:1. In addition, there is a concern that the temperature of the selective mirrors may increase owing to material absorption at longer wavelengths and that the thermal emission from the mirror may degrade the overall device performance.

Here, we propose nanostructured intrinsic semiconductor–based thermal emitters in which the electron thermal fluctuations are first limited to the higher-frequency side of the spectrum, above the semiconductor bandgap, and are then enhanced by the photonic resonance of the structure. This double-resonance approach yields highly selective thermal emission on the shorter-wavelength side. Our theoretical calculations indicated that intrinsic Si rod-array emitters with a rod radius of 105 nm (190 nm) can convert 59% (84%) of the input power into emission shorter than 1100 nm (1800 nm) at 1400 K. We fabricated a Si rod-array emitter exhibiting a high peak emissivity of 0.77 at a wavelength of 790 nm and a low background emissivity of <0.02 to 0.05 for the 1100- to 7000-nm wavelength range, under operation at 1273 K.

RESULTS

According to Kirchhoff's radiation law (*25*), the absorptivity of a material is equal to its emissivity, which implies that the thermal emission spectrum of an emitter can be modified by tailoring its absorption characteristics. In our approach, the emissivity (or absorptivity) spectrum is controlled using both electronic and photonic resonances.

[1]Department of Electronic Science and Engineering, Kyoto University, Kyoto 615-8510, Japan. [2]Energy Technology Laboratories, Osaka Gas Co. Ltd., 6-19-9 Torishima, Konohana-Ku, Osaka 554-0051, Japan. [3]Hakubi Center, Kyoto University, Yoshida, Kyoto 606-8501, Japan.
*Corresponding author. Email: tasano@qoe.kuee.kyoto-u.ac.jp
†These authors contributed equally to this work.

The former approach implies that a material with an appropriate absorption coefficient spectrum should be selected. In the case of thermal emission control in the mid-infrared range, utilization of intersubband transitions in n-doped GaAs/AlGaAs quantum wells has been successful (*3*, *9*, *11*, *12*), but this approach cannot be applied in the near-infrared–to–visible range because of limitations related to the transition wavelength and operating temperature (see the Supplementary Materials for details). Here, we used interband transitions of intrinsic Si (melting point, 1687 K) to establish control of electronic resonance in the near-infrared–to–visible range at temperatures above 1000 K (see fig. S1). We calculated the absorption coefficient spectra of intrinsic Si at various temperatures, considering both interband transitions and free-carrier absorption due to the intrinsic carriers generated at elevated temperatures (see fig. S2). We confirmed that the spectra exhibited a step-like increase at wavelengths shorter than 1.2 to 1.5 μm, even at temperatures above 1000 K (see the Supplementary Materials for details), which is desirable for near-infrared–to–visible selective emitters with suppressed emission at longer wavelengths. To control the photonic resonance, we used an array of rod-type resonators (see Fig. 1A, inset). Rod-type resonators reduce the Si filling factor, which is important for the suppression of nonresonant longer-wavelength emission from the intrinsic free carriers generated at elevated temperatures. We chose a square-lattice array to decrease the interaction between the rods, such that the angular dependence of the emission wavelength was reduced, and to decrease the Si filling factor.

We then calculated the absorptivity (emissivity) spectrum of the Si rod-array structure using the rigorous coupled-wave analysis method (*26*), considering the temperature dependence of the absorption coefficient and the refractive index. The structure was tuned by adjusting the lattice constant a, rod height h, rod radius r, and Si film thickness t_{Si}. Figure 1A shows the spectral emissivity of a Si rod-array emitter in the surface normal direction at 1400 K, with structural parameters a = 500 nm, h = 450 nm, r = 110 nm, and t_{Si} = 50 nm. An emissivity peak of close to unity is apparent at 950 nm, and emissivity at longer wavelengths is strongly suppressed (~0.1 at 1100 nm and <0.015 for wavelengths >1500 nm). The corresponding spectral radiance is shown in Fig. 1B where a large contrast between the intensities below and above 1100 nm is observed. The angular dependence of the emission is plotted in Fig. 1C, and it is apparent that the primary emission range has no strong dependence on the radiation angle. The resonant behavior of the emitter is considered to be mainly determined by the Mie resonances of the Si rods. The total emission spectrum integrated over the upper hemisphere is more important for evaluating the energy utilization efficiency, which is indicated by the solid black line in Fig. 1D. The radiation power density integrated over wavelengths shorter than 1100 nm is 1640 W/m^2, which corresponds to 38% of the total emission power. This means that 38% of the power delivered to the emitter is reemitted as an emission component of <1100 nm when other losses (thermal conduction, convection, and radiation from areas other than the Si nanorods) can be completely suppressed.

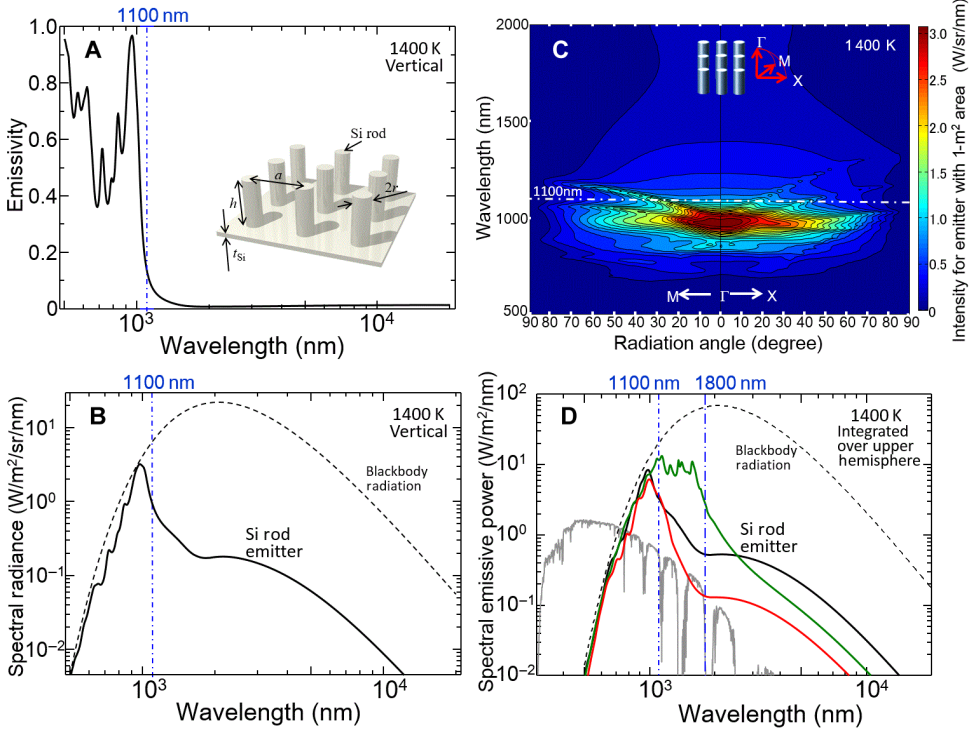

Fig. 1. Theoretical calculation results. (**A**) Spectral emissivity and (**B**) spectral radiance of Si rod-array emitter (solid lines) in the direction normal to the surface at 1400 K with a = 500 nm, h = 450 nm, r = 110 nm, and t_{Si} = 50 nm. The inset in (A) illustrates the emitter structure and parameters. (**C**) Radiation angle dependence of emission intensity at 1400 K for the emitter with a 1-m^2 area. (**D**) Radiation spectra of Si rod-array emitters at 1400 K integrated over the upper hemisphere with structural parameters a = 500 nm, h = 450 nm, r = 110 nm, and t_{Si} = 50 nm (solid black line); a = 600 nm, h = 600 nm, r = 105 nm, and t_{Si} = 0 nm (solid red line); and a = 700 nm, h = 800 nm, r = 190 nm, and t_{Si} = 0 nm (solid green line). The blackbody spectrum at 1400 K integrated over the upper hemisphere (dashed line) and the irradiance of sunlight at AM1.5G (gray line) are also plotted.

The longer-wavelength component is considered to originate from free-carrier absorption/emission by the intrinsic carriers in high-temperature Si (see fig. S2). To suppress this component, we explored the parameter space and obtained a structure that produces a sufficiently strong photonic resonance near 1000 nm with a reduced Si filling factor. This structure (a = 600 nm, h = 600 nm, r = 105 nm, and t_{Si} = 0 nm) yields the emission spectrum indicated by the solid red line in Fig. 1D, where the emission at wavelengths longer than 1100 nm is significantly reduced compared to that of the first structure (black line). The spectrally integrated radiation power density of the second structure for wavelengths shorter than 1100 nm is 1270 W/m^2, which corresponds to 59% of the total emission power. [We also confirmed that the utilization of doped Si with a doping density exceeding the intrinsic carrier density at the operating temperature severely degrades the energy utilization efficiency of the emitter (see fig. S3 and table S1).]

These emitters are suitable for use in S-TPV systems with small absorbers/heaters (*21*) incorporating Si solar cells (bandgap wavelength, ~1100 nm). In addition, we also designed an emitter optimized for GaSb solar cells (bandgap wavelength, ~1800 nm), with structural parameters a = 700 nm, h = 800 nm, r = 190 nm, and t_{Si} = 0 nm. The corresponding emission spectrum is indicated by the solid green line in Fig. 1D. For this device, the spectrally integrated radiation power density for wavelengths shorter than 1800 nm is 7670 W/m^2 at 1400 K, which is 84% of the total radiation power density. Note that these radiation powers are values integrated over the upper hemisphere, and the usable radiation power can be doubled if the emission to both sides is used.

Encouraged by the above theoretical results, we fabricated Si rod-array emitters and measured their thermal emission characteristics. We prepared silicon-on-insulator (SOI) substrates with a 500-nm-thick top Si layer and a 1-μm-thick SiO_2 layer on a 700-μm-thick Si substrate. Rod-array patterns were formed on a 1-mm × 1-mm region of the top Si film using electron beam lithography and plasma etching techniques (see Materials and Methods). Three samples with r values of 85, 90, and 105 nm were fabricated; the other parameters were identical for each sample (a = 600 nm, h = 500 nm, and t_{Si} = 0 nm). Note that h was 500 nm rather than 600 nm because of a limitation of the prepared SOI substrate. Figure 2A shows a scanning electron microscope image of a fabricated sample with r = 105 nm. An array of Si rods with good verticality and a high aspect ratio of >2.3 was fabricated. The thick Si substrate underneath the Si rod-array area was removed to reduce the background emission; however, a thin SiO_2 film (t_{SiO2} = 1000 nm) was left in place to support the Si rod array.

Optical measurements were conducted using a microscope-based spectroscopy system (see Materials and Methods). The red lines in Fig. 2B show the near-infrared emissivity spectra of the samples at 1273 K, as observed in the surface normal direction. In this figure, the main emissivity peaks of the samples with r values of 105, 90, and 85 nm are at 915, 870, and 790 nm, respectively. For the sample with r = 105 nm, the peak emissivity at 915 nm is 0.62, whereas the emissivity at 1100 to 1400 nm is only 0.02 to 0.04. In addition, for the sample with r = 90 nm, the peak emissivity at 870 nm is 0.78, whereas the emissivity at 1100 to 1400 nm is only 0.02 to 0.04. Finally, for the sample with r = 85 nm, the peak emissivity at 790 nm is 0.77, with the emissivity at 1000 to 1100 nm being only 0.02 to 0.04. The blue lines in Fig. 2B represent the theoretical emissivity spectra calculated for each sample, which are in agreement with the experimental spectra. Sharp peaks in theoretical calculations are considered to be averaged

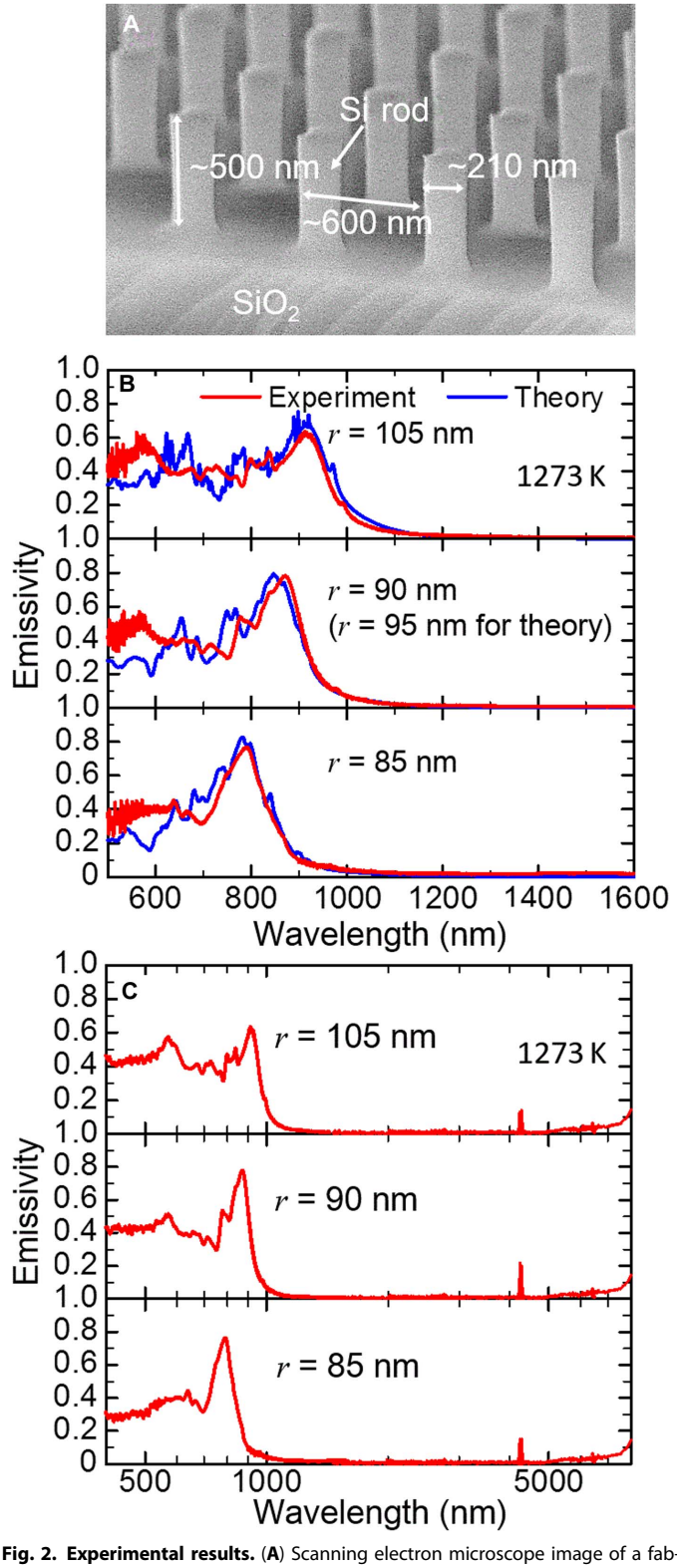

Fig. 2. Experimental results. (**A**) Scanning electron microscope image of a fabricated sample with r = 105 nm. (**B**) Measured thermal emissivity of Si rod arrays (solid red lines) with r values of 105, 90, and 85 nm at 1273 K in surface normal direction in the near-infrared range. The theoretically calculated emissivity spectra are indicated by solid blue lines. (**C**) Measured wide-range emissivity spectra of Si rod arrays at 1273 K. The emissivity peak at 4200 nm is due to absorption by CO_2.

out in the experiment because of fluctuations of the fabricated structures. On the basis of this agreement, it is expected that the experimental emission spectrum integrated for the upper hemisphere will be similar to the theoretical results shown in Fig. 1D.

Figure 2C shows the corresponding wide-range emissivity spectra, where the data in the mid-infrared range (1600 to 8000 nm) were measured using a Fourier transform infrared (FTIR) spectrometer. The emissivity is strongly suppressed to values below 0.02 for 1200 to 4800 nm and below 0.05 for 4800 to 7000 nm. The emissivity peak at 4200 nm is due to the absorption lines of the CO_2 in the surrounding air. Note that the increase in the emissivity at wavelengths greater than 4800 nm is due to the 1000-nm-thick SiO_2 layer supporting the Si rods (see the SiO_2 absorption spectrum in fig. S2). This emission can be avoided by using a transparent substrate, such as sapphire or MgO. Note that no such problems are apparent in the emissivity spectrum tail on the short-wavelength side. This is because the actual emission intensity here is cropped by the blackbody radiation tail, as shown in Fig. 1 (B to D).

DISCUSSION

The results obtained here demonstrate that simultaneous utilization of the Si electronic interband resonance and the photonic resonance of the rod-array structure facilitates the realization of highly selective and tunable near-infrared–to–visible thermal emitters. Although the emitters investigated here have a surface area of 1 mm^2, these simple rod-array patterns can be scaled to larger areas using nanoimprint lithography techniques and transparent substrates. In addition, the durability of the emitters can be increased by coating Si rods with thin Al_2O_3 using an atomic layer deposition technique.

CONCLUSION

We investigated selective thermal emitters that use the Si interband transition and the optical resonance of rod arrays with a small material filling factor. For a rod radius of 85 nm, our fabricated Si rod-array emitters exhibit a high emissivity of 0.77 at a wavelength of 790 nm for the vertical direction, along with a low emissivity of <0.02 to 0.05 in the 1100- to 7000-nm wavelength range at 1273 K. When the rod radius is 105 nm, the experimental emissivity is 0.62 at a wavelength of 915 nm and <0.02 to 0.05 for the 1200- to 7000-nm wavelength range. In addition, theoretical calculations showed that optimized Si rod-array emitters with a rod radius of 105 nm (190 nm) can convert 59% (84%) of the input power into emission at wavelengths shorter than 1100 nm (1800 nm) at 1400 K. We believe that our approach constitutes a promising new route toward thermal emission control and that this method can be extended to deep within the visible range by using other semiconductors with a higher bandgap and the ability to withstand higher temperatures, including SiC. Moreover, the combination of our approach and the selective-mirror approach (*13*–*16*) will yield a large synergetic effect on the improvement of energy utilization efficiency because this will allow the temperature increase of the mirror to be suppressed significantly.

MATERIALS AND METHODS

Materials

We prepared SOI substrates with a 500-nm-thick top Si layer and a 1000-nm-thick SiO_2 layer on a 700-μm-thick Si substrate. After the top Si layer was coated with an electron beam resist (ZEP520A), rod-array patterns with areas of 1 mm × 1 mm were drawn using electron beam lithography, in which the patterns were transferred to the top Si layer via an SF_6-based plasma etching process. Next, the bottom Si substrate was ground to a thickness of 100 μm, and the residual Si substrate under the rod array was removed using a dry etching process over a 2.4-mm-diameter area. This procedure was necessary to avoid thermal emission from the Si substrate.

Methods

The optical measurements were conducted using a microscope-based spectroscopy system. The sample was placed on a ceramic heater in an Ar-filled (~800 Pa) chamber. The heater had a 1.8-mm-diameter hole in the center, and the position of the rod-array area of the sample was adjusted relative to the hole to avoid observation of the heater emission. The sample emission was collected by a BaF_2 lens with an effective numerical aperture of 0.05. An image of a 400-μm-diameter portion of the emitter area was selected using a pinhole situated at the intermediate focal plane. This image was then transferred to a grating-type spectrometer equipped with Si and InGaAs detector arrays or to an FTIR spectrometer equipped with an HgCdTe detector. All detectors were cooled with liquid nitrogen. The observable wavelength ranges were 500 to 1100 and 900 to 1600 nm for the spectrometer with the Si and InGaAs detector arrays, respectively, and 1430 to 8000 nm for the FTIR spectrometer with the HgCdTe detector.

SUPPLEMENTARY MATERIALS

Supplementary material for this article is available at http://advances.sciencemag.org/cgi/content/full/2/12/e1600499/DC1

Material selection

Absorption coefficient of Si

Thermal radiation spectra of n-doped Si rod-array emitters

fig. S1. Spectral irradiance of the sun [air mass 1.5 global (AM1.5G)] and blackbody radiation spectra integrated over a hemisphere at various temperatures.

fig. S2. Theoretical absorption coefficient of Si at various temperatures on a linear scale and a log-log scale.

fig. S3. Theoretical thermal radiation power density spectra of structurally identical Si rod-array emitters with different doping densities at 1400 K.

table S1. Doping density dependence of the energy utilization efficiency of structurally identical Si rod-array emitters.

References (*27*–*30*)

REFERENCES AND NOTES

1. J. F. Waymouth, Where will the next generation of lamps come from? *J. Light Visual Environ.* **13**, 51–68 (1989).
2. R. M. Swanson, A proposed thermophotovoltaic solar energy conversion system. *Proc. IEEE* **67**, 446–447 (1979).
3. T. Inoue, M. De Zoysa, T. Asano, S. Noda, Filter-free nondispersive infrared sensing using narrow-bandwidth mid-infrared thermal emitters. *Appl. Phys. Express* **7**, 012103 (2014).
4. J. G. Fleming, S. Y. Lin, I. El-Kady, R. Biswas, K. M. Ho, All-metallic three-dimensional photonic crystals with a large infrared bandgap. *Nature* **417**, 52–55 (2002).
5. J.-J. Greffet, R. Carminati, K. Joulain, J.-P. Mulet, S. Mainguy, Y. Chen, Coherent emission of light by thermal sources. *Nature* **416**, 61–64 (2002).
6. H. Sai, Y. Kanamori, H. Yugami, High-temperature resistive surface grating for spectral control of thermal radiation. *Appl. Phys. Lett.* **82**, 1685–1687 (2003).
7. F. Kusunoki, J. Takahara, T. Kobayashi, Qualitative change of resonant peaks in thermal emission from periodic array of microcavities. *Electron. Lett.* **39**, 23–24 (2003).
8. K. Ikeda, H. T. Miyazaki, T. Kasaya, K. Yamamoto, Y. Inoue, K. Fujimura, T. Kanakugi, M. Okada, K. Hatade, S. Kitagawa, Controlled thermal emission of polarized infrared waves from arrayed plasmon nanocavities. *Appl. Phys. Lett.* **92**, 021117 (2008).
9. T. Asano, K. Mochizuki, M. Yamaguchi, M. Chaminda, S. Noda, Spectrally selective thermal radiation based on intersubband transitions and photonic crystals. *Opt. Express* **17**, 19190–19203 (2009).

10. X. Liu, T. Tyler, T. Starr, A. F. Starr, N. M. Jokerst, W. J. Padilla, Taming the blackbody with infrared metamaterials as selective thermal emitters. *Phys. Rev. Lett.* **107**, 045901 (2011).
11. M. De Zoysa, T. Asano, K. Mochizuki, A. Oskooi, T. Inoue, S. Noda, Conversion of broadband to narrowband thermal emission through energy recycling. *Nat. Photonics* **6**, 535–539 (2012).
12. T. Inoue, M. De Zoysa, T. Asano, S. Noda, Single-peak narrow-bandwidth mid-infrared thermal emitters based on quantum wells and photonic crystals. *Appl. Phys. Lett.* **102**, 191110 (2013).
13. H. Kostlin, F. H. R. Almer, Incandescent lamp with infrared filter. U.S. Patent 4,017,758 (1977).
14. I. S. Goldstein, R. P. Fontana, L. Thorington, R. P. Howson, The design, construction and performance of an incandescent light source with a transparent heat mirror. *Lighting Res. Technol.* **18**, 93–97 (1986).
15. R. S. Bergman, Halogen-IR lamp development: A system approach. *J. Illum. Eng. Soc.* **20**, 10–16 (1991).
16. O. Ilic, P. Bermel, G. Chen, J. D. Joannopoulos, I. Celanovic, M. Soljačić, Tailoring high-temperature radiation and the resurrection of the incandescent source. *Nat. Nanotechnol.* **11**, 320–324 (2016).
17. E. Rephaeli, S. Fan, Absorber and emitter for solar thermo-photovoltaic systems to achieve efficiency exceeding the Shockley-Queisser limit. *Opt. Express* **17**, 15145–15159 (2009).
18. Y. X. Yeng, M. Ghebrebrhan, P. Bermel, W. R. Chan, J. D. Joannopoulos, M. Soljačić, I. Celanovic, Enabling high-temperature nanophotonics for energy applications. *Proc. Natl. Acad. Sci. U.S.A.* **109**, 2280–2285 (2012).
19. C. Wu, B. Neuner III, J. John, A. Milder, B. Zollars, S. Savoy, G. Shvets, Metamaterial-based integrated plasmonic absorber/emitter for solar thermo-photovoltaic systems. *J. Opt.* **14**, 024005 (2012).
20. H. Kobayashi, J. Sakai, A. Kohiyama, M. Shimizu, F. Iguchi, H. Yugami, A solar thermophotovoltaic generation with a monolithic planar absorber/emitter material. *J. Renew. Energy Environ.* **2013**, JM3A.20 (2013).
21. A. Lenert, D. M. Bierman, Y. Nam, W. R. Chan, I. Celanović, M. Soljačić, E. N. Wang, A nanophotonic solar thermophotovoltaic device. *Nat. Nanotechnol.* **9**, 126–130 (2014).
22. Y. X. Yeng, W. R. Chan, V. Rinnerbauer, V. Stelmakh, J. J. Senkevich, J. D. Joannopoulos, M. Soljacic, I. Čelanović, Photonic crystal enhanced silicon cell based thermophotovoltaic systems. *Opt. Express* **23**, A157–A168 (2015).
23. E. Rephaeli, A. Raman, S. Fan, Ultrabroadband photonic structures to achieve high-performance daytime radiative cooling. *Nano Lett.* **13**, 1457–1461 (2013).
24. B. J. O'Regan, Y. Wang, T. F. Krauss, Silicon photonic crystal thermal emitter at near-infrared wavelengths. *Sci. Rep.* **5**, 13415 (2015).
25. D. B. Brace, *The Laws of Radiation and Absorption: Memoirs by Prévost, Stewart, Kirchhoff, and Kirchhoff and Bunsen* (American Book Company, 1901).
26. Z.-Y. Li, L.-L. Lin, Photonic band structures solved by a plane-wave-based transfer-matrix method. *Phys. Rev. E* **67**, 046607 (2003).
27. H. D. Barber, Effective mass and intrinsic concentration in silicon. *Solid State Electron.* **10**, 1039–1051 (1967).
28. C. J. Fu, Z. M. Zhang, Nanoscale radiation heat transfer for silicon at different doping levels. *Int. J. Heat Mass Transfer* **49**, 1703–1718 (2006).
29. H. Rogne, P. J. Timans, H. Ahmed, Infrared absorption in silicon at elevated temperatures. *Appl. Phys. Lett.* **69**, 2190–2192 (1996).
30. J. Kischkat, S. Peters, B. Gruska, M. Semtsiv, M. Chashnikova, M. Klinkmüller, O. Fedosenko, S. Machulik, A. Aleksandrova, G. Monastyrskyi, Y. Flores, W. T. Masselink, Mid-infrared optical properties of thin films of aluminum oxide, titanium dioxide, silicon dioxide, aluminum nitride, and silicon nitride. *Appl. Opt.* **51**, 6789–6798 (2012).

Acknowledgments: We thank T. Inoue and K. Ishizaki for fruitful discussions. **Funding:** This work was supported in part by Japan Society for the Promotion of Science Grant-in-Aid for Scientific Research (KAKENHI) grant no. 25220607 and the Super Cluster Program of the Japan Science and Technology Agency. **Author contributions:** T.A. and S.N. designed the study. T.S. performed the analyses. M.S., K.H., and M.D.Z. performed the analyses and experiments. T.T. conducted the experiments. All authors participated in discussing the results. **Competing interests:** The authors declare that they have no competing interests. **Data and materials availability:** All data needed to evaluate the conclusions in the paper are present in the paper and/or the Supplementary Materials. Additional data related to this paper may be requested from the authors.

Submitted 8 March 2016
Accepted 15 November 2016
Published 23 December 2016
10.1126/sciadv.1600499

Citation: T. Asano, M. Suemitsu, K. Hashimoto, M. De Zoysa, T. Shibahara, T. Tsutsumi, S. Noda, Near-infrared–to–visible highly selective thermal emitters based on an intrinsic semiconductor. *Sci. Adv.* **2**, e1600499 (2016).

Science Advances

Near-infrared–to–visible highly selective thermal emitters based on an intrinsic semiconductor

Takashi Asano, Masahiro Suemitsu, Kohei Hashimoto, Menaka De Zoysa, Tatsuya Shibahara, Tatsunori Tsutsumi and Susumu Noda

Sci Adv **2** (12), e1600499.
DOI: 10.1126/sciadv.1600499